Silicon-Based Peripheral Steric Donor Modifications for High-Efficiency Multi-Resonance Thermally Activated Delayed Fluorescence Emitter

Hai-Tian Yuan,‡[a,b] Yue-Jian Yang,‡[a,b] Zhe-Hong Yu,[a,b] Qi Zheng,[a,b] Hong-Yan Yan,[a,b] Yu Wang,[a,b] Dong-Ying Zhou, *[a,b] Liang-Sheng Liao[a,b,c] and Zuo-Quan Jiang*[a,b]

a. Institute of Functional Nano & Soft Materials (FUNSOM), Joint International Research Laboratory of Carbon-Based Functional Materials and Devices, Soochow University, Suzhou, 215123, Jiangsu, PR China.

b. Jiangsu Key Laboratory for Carbon-Based Functional Materials & Devices, Soochow University, Suzhou, 215123, Jiangsu, PR China.

c. Macao Institute of Materials Science and Engineering Macau University of Science and Technology 999078 Taipa, Macau SAR (China).

‡These authors contribute equally to this work.

All chemicals and reagents were used as received from commercial resources without further purification. ^{1}H NMR and ^{13}C NMR spectra were measured on a Bruker 400 at room temperature. Matrix-assisted laser desorption/ionization time-of-flight mass spectrometry (MALDI-TOF-MS) was performed on Bruker Autoflex II/Compass 1.0. UV–vis absorption spectra were recorded on a Shimadzu UV 2600 spectrophotometer. Photoluminescence (PL) spectra and phosphorescent spectra were performed on Hitachi F-4600 fluorescence spectrophotometer or Horiba JY FL-3 fluorescence spectrophotometer. The PLQY values were measured using Hamamatsu C9920-02G in an integrating sphere under a nitrogen atmosphere. The PLQY measurement range can cover from 300 nm to 950 nm. Transient spectra were obtained by using the Quantaurus-Tau fluorescence lifetime measurement system (C11367-03, Hamamatsu Photonics Co.) in the vacuum. Thermogravimetric analysis (TGA) was performed on TA SDT 2960 instrument at a heating rate of 10 °C/min under nitrogen, the temperature at 5% weight loss was used as the decomposition temperature (T_d). The electrochemical measurement was made using a CHI760 voltammetric analyzer. A conventional three-electrode configuration consisting of a platinum working electrode, a Pt-wire counter electrode, and an Ag/AgCl reference electrode was used. The solvent in the measurement was CH_2Cl_2, and the supporting

electrolyte was 0.1 M tetrabutylammonium hexafluorophosphate. Ferrocene was added as a calibrant after each set of measurements, and all potentials reported were quoted regarding the ferrocene-ferrocenium (Fc/Fc^+) couple $E(Fc/Fc^+)$ at a scan rate of 100 mV/s. All DFT calculation was carried out using the Gaussian 16 C.01 software package. [1] The gas-phase ground state geometry optimizations were performed at B3LYP/6-31G(d, p) level with the ω value of 0.3. [2] Then TD-DFT calculation was adopted at ω-tuned ωb97xd/ def2-SVP level to optimize the geometries of excited states. [3,4] Based on the results of TD-DFT calculation, hole-electron analysis was performed using Multiwfn 3.8 software package and VMD 1.9.3. [5,6] IGMH analysis [7] was performed using Multiwfn 3.8 software package [6] and VMD 1.9.3[5].

Single-crystal information.

The crystals of BNSi was grown by slow evaporation in dichloromethane and ethano. Data collection was accomplished on a Bruker APEX-II CCD' diffractometer with a Turbo X-ray Source (Mo–Kα radiation, $\lambda = 0.71073$ Å) adopting the direct-drive rotating anode technique and a CMOS detector. Using Olex2, the structure was solved with the ShelXT structure solution program using Intrinsic Phasing and refined with the ShelXL refinement package using Least Squares minimization. The X-ray crystallographic coordinates for the structure reported in this study have been deposited at the Cambridge Crystallographic Data Centre (CCDC), under deposition number 2369645 (BNSi). These data can be obtained free of charge from The Cambridge Crystallographic Data Centre "http://www.ccdc.cam.ac.uk/data_request/cif".

OLED fabrication and measurements.

OLEDs were fabricated on an ITO glass substrate layer (110 nm, 15 Ω/square) under a base pressure of 3×10^{-6} Torr. The active area of each device is 0.09 cm^2. Deposition rates and thicknesses of all materials were monitored with oscillating quartz crystals. Doping layers were deposited by utilizing two different sensors to monitor the deposition rates of both host material and dopant material. The deposition rate of the host was controlled at 0.2 nm s^{-1}, and the deposition rate of the dopant was adjusted according to the volume ratio doped in the host materials. The electroluminescence (EL) and current density-voltage(J-V) characteristics of the devices were measured by a constant current source (Keithley 2400 SourceMeter) combined with a photometer (Photo Research SpectraScan PR655).

Synthesis and characterization

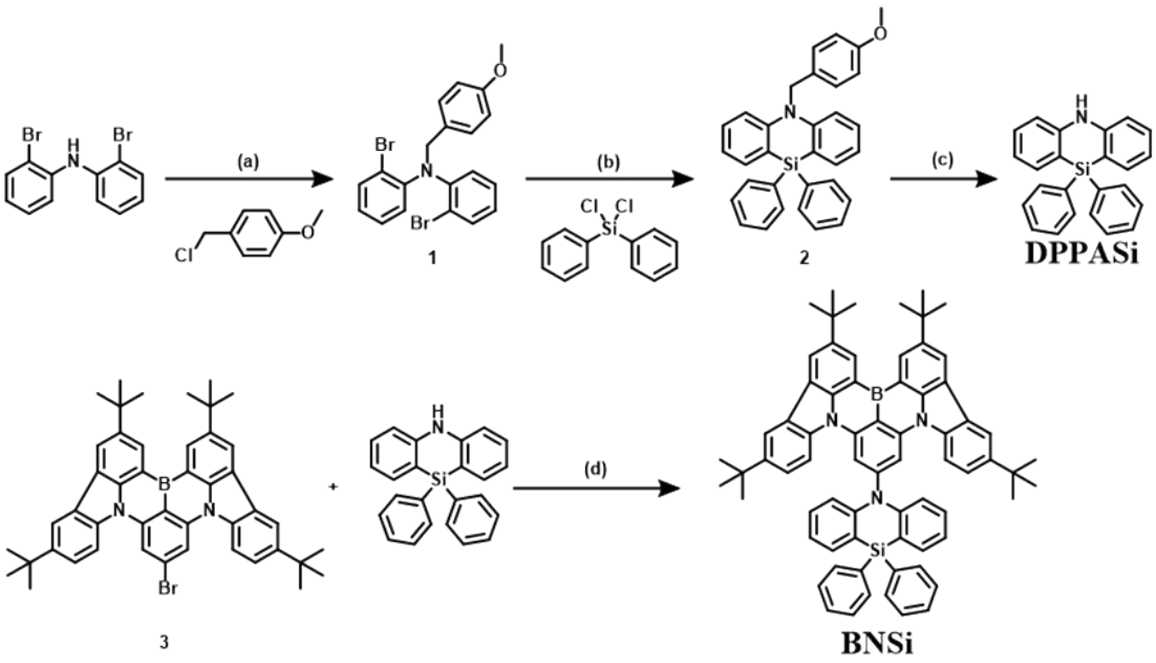

Scheme 1. Synthetic routes of BNSi. (a) NaH, DMF, room temperature, 15 h; (b) *n*-BuLi, THF, 0 ˚C, 1 h then dichlorodiphenylsilane, room temperature, 16 h; (c) 2,3-Dichloro-5,6-dicyano-1,4-benzoquinone, Tol, H_2O, 80 ˚C, 14 h; (d) $Pd_2(dba)_3$, tri-*tert*-butylphosphine tetrafluoroborate, *t*-BuONa, Tol, 110 ˚C, 16 h.

10,10-diphenyl-5,10-dihydro-dibenzo[b,e][1,4]azasiline (DPPASi) and compound 3 were synthesized according to the literature procedures.[11] All other reagents and solvents are used from commercial sources without further purification.

Synthesis of BNSi

DPPASi (0.53 g, 1.53 mmol), *t*BuCzBN-Br (1.00 g, 1.39 mmol), $Pd_2(dba)_3$ (0.04 g, 0.04 mmol), tri-tert-butylphosphine (0.04 g, 0.14 mmol) and sodium tert-butoxide (0.40 g, 4.17 mmol) were dissolved in 20 mL of toluene in a 50 mL two-neck flask under nitrogen atmosphere. The mixture was stirred and heated at 110 °C for 16 h. After cooling to room temperature, the mixture was concentrated under reduced pressure to remove Tol. The crude product was further purified by column chromatography on silica gel using petroleum ether/dichloromethane (1/3, v/v) as eluent to obtain BNSi (0.56 g) as a yellow solid. Yield: 41%. ^{1}H NMR (400 MHz, Chloroform-d) δ 9.21 (d, *J* = 1.9 Hz, 2H), 8.52 (d, *J* = 1.7 Hz, 2H), 8.27 (d, *J* = 2.0 Hz, 2H), 8.25 (s, 2H), 8.10 (d, *J* = 8.8 Hz, 2H), 7.79 - 7.76 (m, 4H), 7.72 (dd, *J* = 7.3, 1.8 Hz, 2H), 7.56 - 7.46 (m, 8H), 7.27 -7.22 (m, 2H), 7.05 (t, *J* = 7.1 Hz, 2H), 6.94 (d, *J* = 8.6 Hz, 2H), 1.73 (s, 18H), 1.52 (s, 18H). ^{13}C NMR (101 MHz, Chloroform-d) δ 145.66, 145.06, 138.09, 136.21, 135.89, 130.66, 129.65, 128.01, 127.07, 124.63, 123.81, 120.87, 120.66, 118.24, 117.20, 114.19, 35.24, 34.78, 32.20, 31.76. ESI-MS (m/z) of $C_{70}H_{66}BN_3Si$ for $[M]^+$: calcd. 988.21; found, 988.06. Overall yield: 6%.

Crystal data and structure refinement

Table S1. Crystal data and structure refinement of **BNSi** in dichloromethane and ethanol.

Identification code	BNSi
Empirical formula	$C_{70}H_{66}BN_3Si$
Formula weight	988.15
Temperature/K	150
Crystal system	triclinic
Space group	P-1
a/Å	11.7436(3)
b/Å	16.3768(4)
c/Å	16.5371(4)
α/°	81.9350(10)
β/°	79.6900(10)
γ/°	71.3010(10)
Volume/Å^3	2952.18(13)
Z	2
ρ_{calc}g/cm^3	1.112
μ/mm^{-1}	0.668
F(000)	1052.0
Crystal size/mm^3	0.19 × 0.12 × 0.08
Radiation	CuKα (λ = 1.54178)
2Θ range for data collection/°	5.454 to 127.406
Index ranges	-13 ≤ h ≤ 13, -18 ≤ k ≤ 19, -19 ≤ l ≤ 19
Reflections collected	19252
Independent reflections	9596 [R_{int} = 0.0765, R_{sigma} = 0.0973]
Data/restraints/parameters	9596/0/688
Goodness-of-fit on F^2	1.027
Final R indexes [I>=2σ (I)]	R_1 = 0.0722, wR_2 = 0.1853
Final R indexes [all data]	R_1 = 0.0925, wR_2 = 0.2069
Largest diff. peak/hole / e Å^{-3}	0.46/-0.47

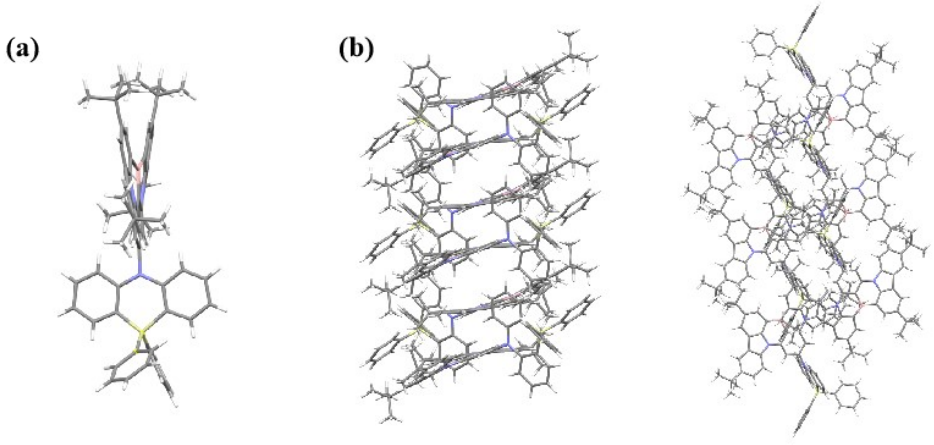

Figure S1. (a) Side view of the single-crystal structures of BNSi; (b) packing mode of BNSi.

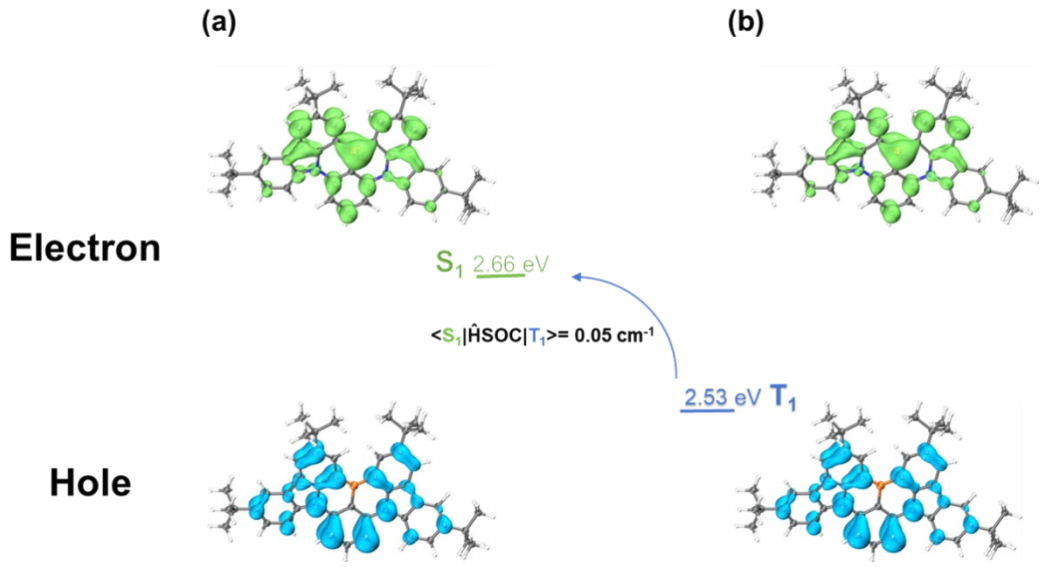

Figure S2. The analysis for the distribution of the hole and electron for the singlet excited states (a) and triplet excited state (b) of DtBuCzB.

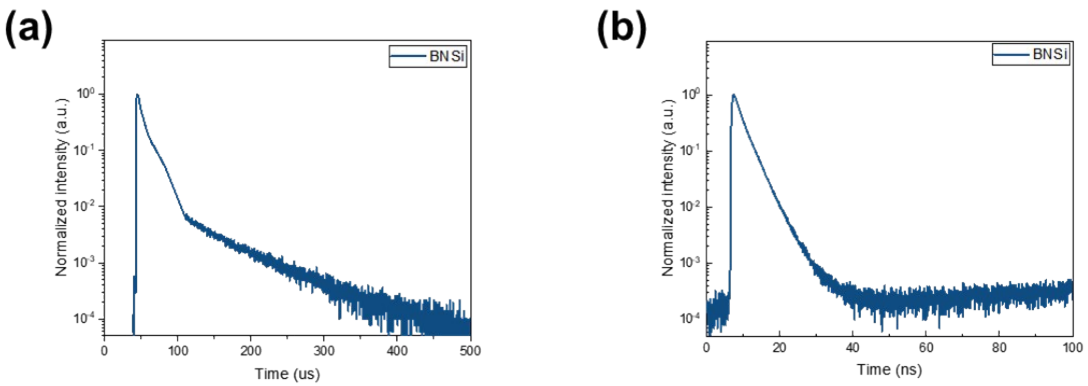

Figure S3. Transient spectra of 15 wt% BNSi in PhCzBCz.

Table S2. Photophysical properties of BNSi in various solvents.

Solvent	**λ_{PL} (nm)**	**FWHM (nm)**
TOL	484	21
THF	484	24
DCM	482	27

DMF	484	29
DMSO	490	37

Table S3. Photophysical properties of BNSi in doped PhCzBCz films (15 wt%)

Compound	Φ_{PF}/Φ_{DF} %/%	τ_{PF}/τ_{DF} ns/μs	k_{PF} (10^8 s^{-1})	k_{DF} (10^4 s^{-1})	k_r (10^7 s^{-1})	k_{ISC} (10^8 s^{-1})	k_{RISC} (10^5 s^{-1})
BNSi	35.6/62.4	8.5/90	1.18	1.11	1.16	1.15	1.01

In this work, the doped films of **BNSi** do not exhibit phosphorescence emission at 300 K. In other words, the efficiency of phosphorescence is zero (Φ_{Phos} = 0). Thus, the quantum efficiency of delayed emission (Φ_{DE}) is equal to the efficiency of delayed fluorescence (Φ_{DF}). Thus, the quantum efficiencies of prompt (Φ_{PF}) and delayed emission (Φ_{DF}) are evaluated by the corrected estimation method and the rate constants were calculated according to the reported method.[8-10]

$$k_{PF} = \frac{1}{\tau_{PF}}$$

$$k_{DF} = \frac{1}{\tau_{DF}}$$

$$k_r^S = k_{PF}\Phi_{PF}$$

$$k_{nr}^S = k_{PF}\frac{\Phi_{PF}}{\Phi_{all}}(1 - \Phi_{all})$$

$$k_{ISC} = k_{PF}\frac{\Phi_{DF}}{\Phi_{all}} - k_{DF}\frac{\Phi_{DF}}{\Phi_{PF}}$$

$$k_{RISC} = k_{DF}\frac{\Phi_{all}}{\Phi_{PF}}$$

$$k_{nr}^T = 0$$

where k_{PF} and k_{DF} are the radiative decay rate for prompt and delayed fluorescence, respectively; Φ_{all} is the total photoluminescence quantum efficiency; k_r^S and k_{nr}^S are the radiative and nonradiative decay rate constants from a singlet excited state, respectively; k_{ISC} and k_{RISC} are the intersystem crossing and reverse intersystem crossing rate constants, respectively; k_{nr}^T is the nonradiative decay rate constant from a triplet excited state.

Table S4. PLQY of BNSi in doped PhCzBCz films.

Doping ratio (wt%)	PLQY(%)
5	95

10	98
15	99
20	94

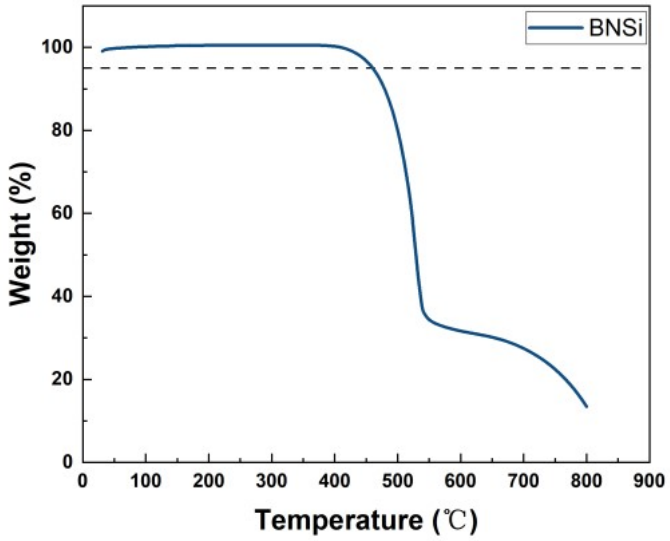

Figure S4. TGA curve of BNSi.

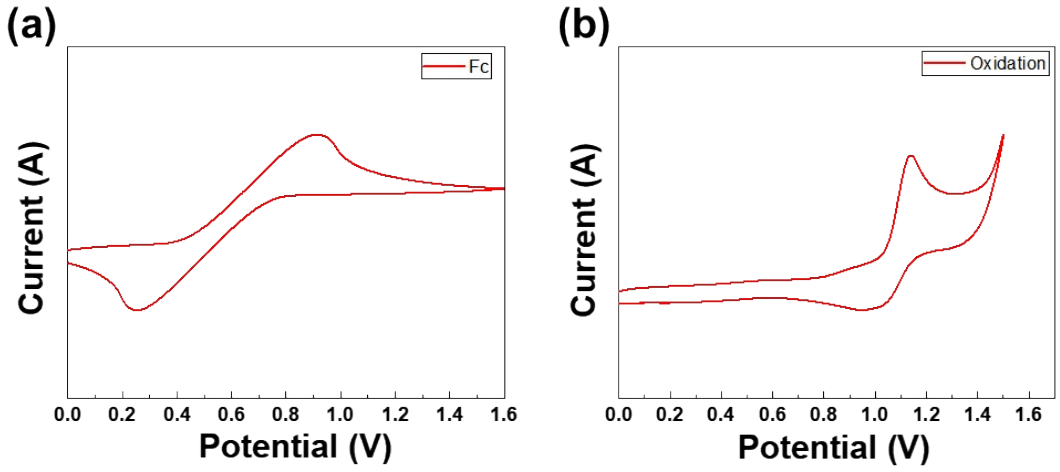

Figure S5. CV curves of ferrocene (a) and BNSi (b).

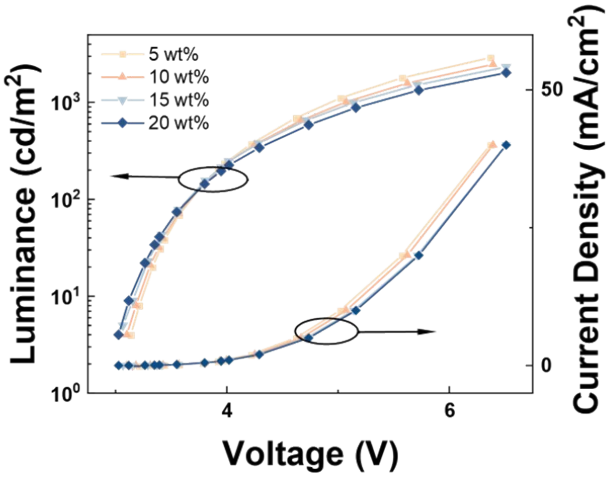

Figure S6. J-V-L curves of BNSi.

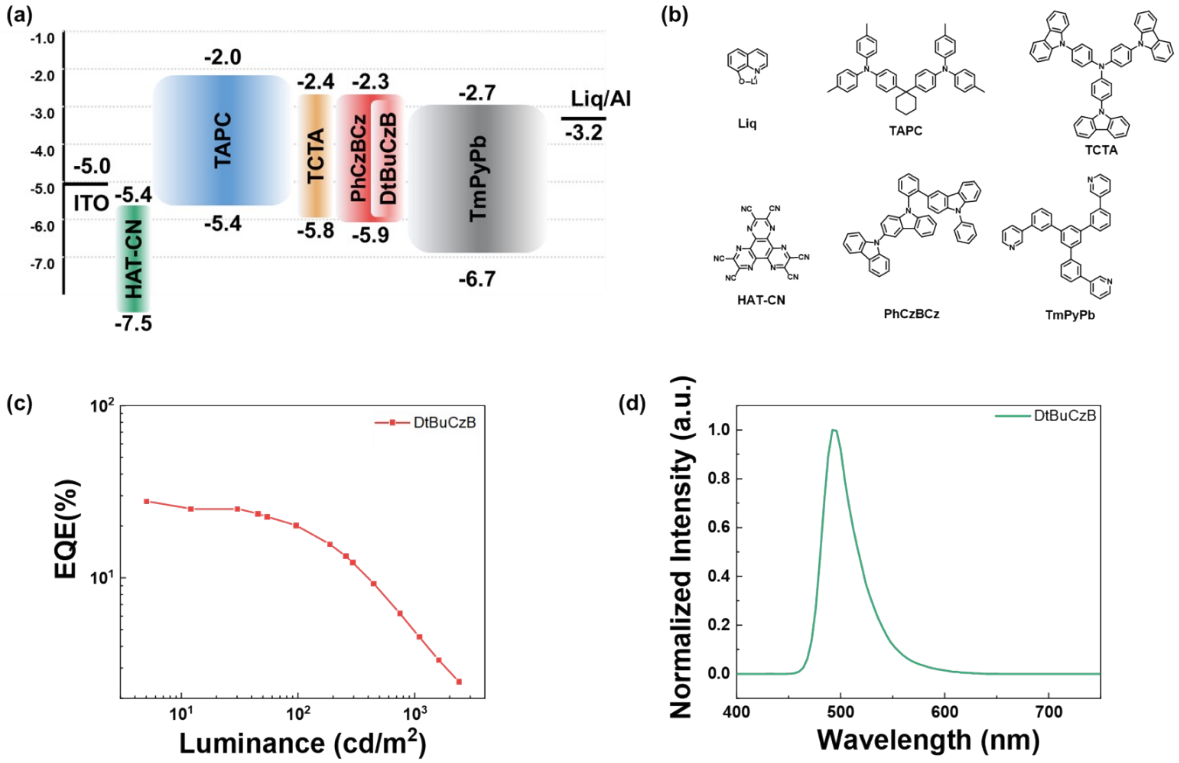

Figure S7. (a) Device structures of OLEDs and (b)chemical structures of the used materials; (c) EQE-luminance (EQE-L) curves of the OLED devices; (d) PL spectra.

Table S5. Summary of OLED device performance of DtBuCzB.

Emitters	X (wt%)	V_{on}[(a)] (V)	FWHM[(b)] (nm)	λ_{EL}[(c)] (nm)	CE[(d)] (cd A^{-1})	EQE[(e)] (%)

DtBuCzB/PhCzBCz	15	3.1	36	494	60.4	27.4/20.2/4.9

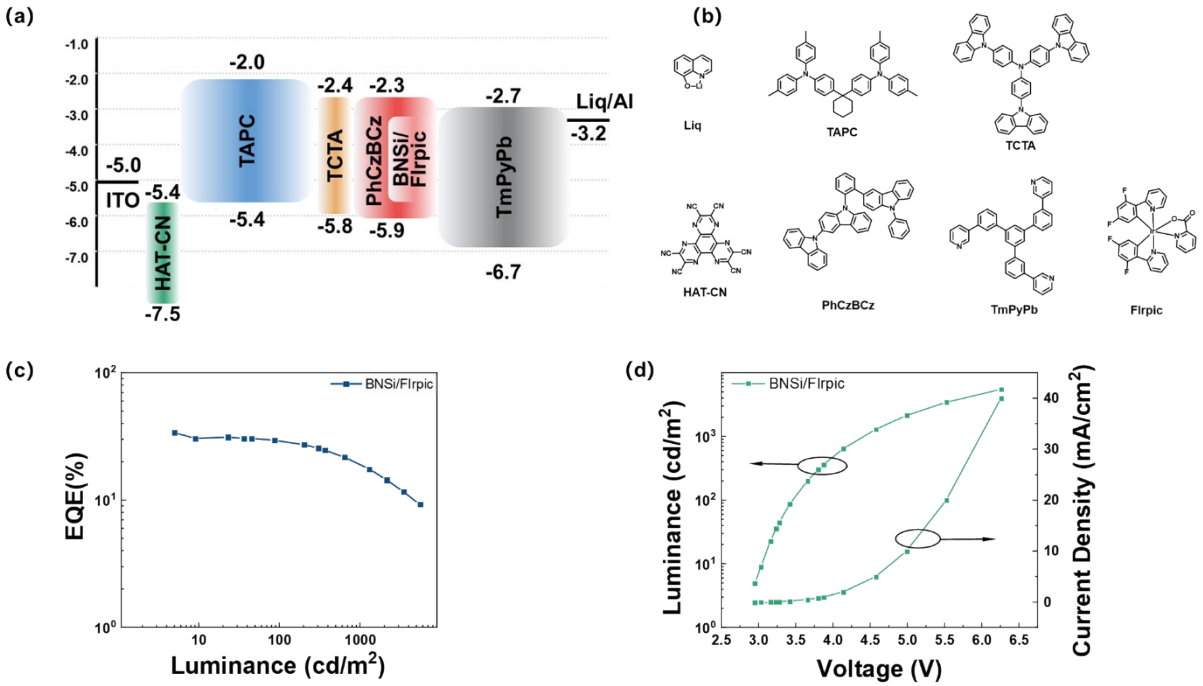

Figure S8. (a) Device structures of OLEDs and (b)chemical structures of the used materials; (c) EQE-luminance (EQE-L) curve of the OLED device;(d) J-V-L curve.

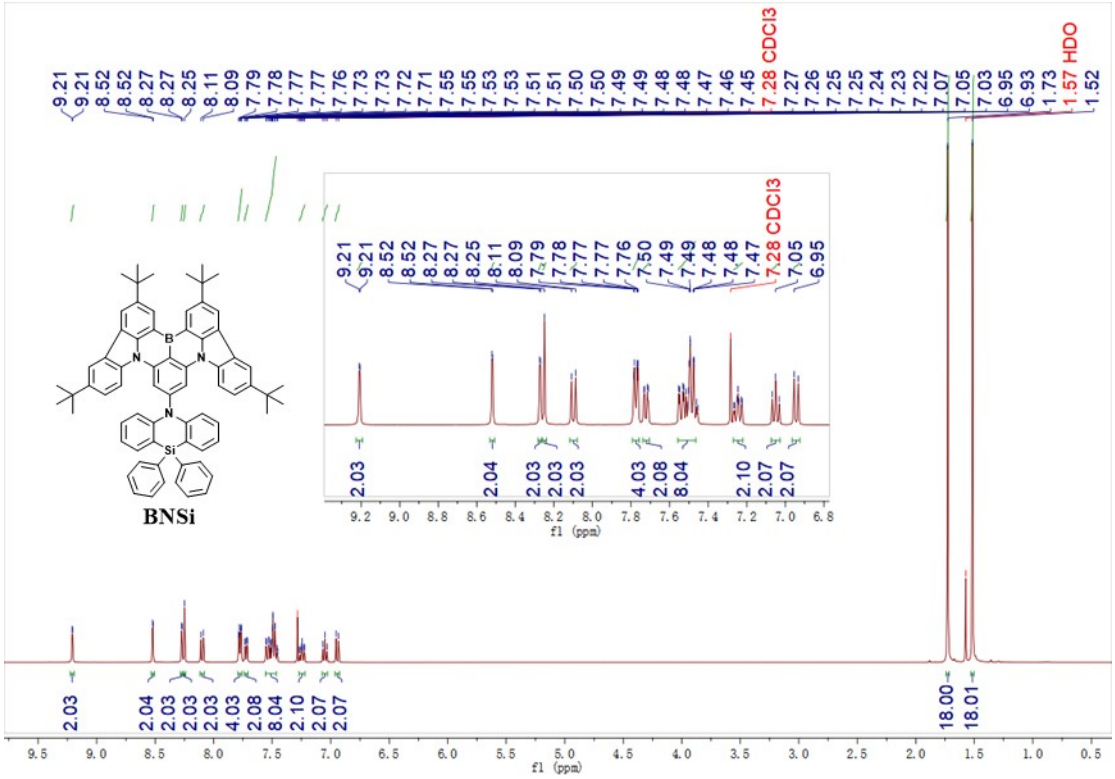

Figure S9. ^{1}H NMR spectrum of BNSi.

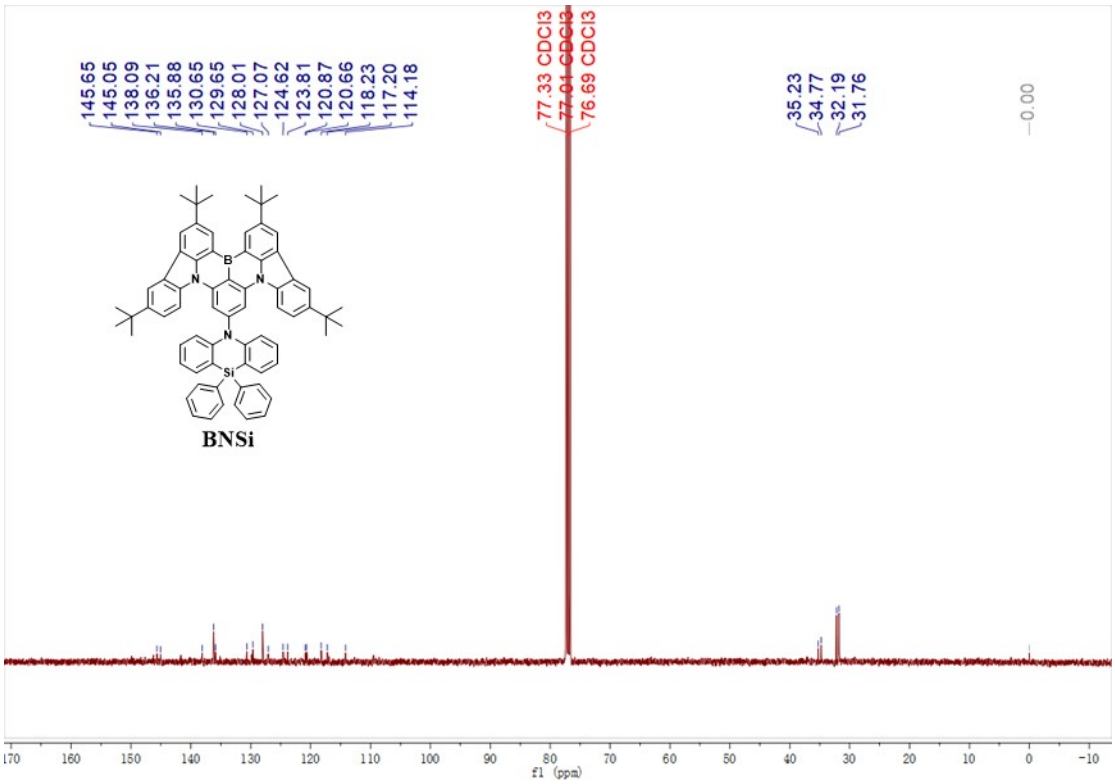

Figure S10. ^{13}C NMR spectrum of BNSi.

Reference

(1) M. J. Frisch, G. W. Trucks, H. B. Schlegel, G. E. Scuseria, M. A. Robb, J. R. Cheeseman, G. Scalmani, V. Barone, G. A. Petersson, H. Nakatsuji, X. Li, M. Caricato, A. V. Marenich, J. Bloino, B. G. Janesko, R. Gomperts, B. Mennucci, H. P. Hratchian, J. V. Ortiz, A. F. Izmaylov, J. L. Sonnenberg, Williams, F. Ding, F. Lipparini, F. Egidi, J. Goings, B. Peng, A. Petrone, T. Henderson, D. Ranasinghe, V. G. Zakrzewski, J. Gao, N. Rega, G. Zheng, W. Liang, M. Hada, M. Ehara, K. Toyota, R. Fukuda, J. Hasegawa, M. Ishida, T. Nakajima, Y. Honda, O. Kitao, H. Nakai, T. Vreven, K. Throssell, J. A. Montgomery Jr., J. E. Peralta, F. Ogliaro, M. J. Bearpark, J. J. Heyd, E. N. Brothers, K. N. Kudin, V. N. Staroverov, T. A. Keith, R. Kobayashi, J. Normand, K. Raghavachari, A. P. Rendell, J. C. Burant, S. S. Iyengar, J. Tomasi, M. Cossi, J. M. Millam, M. Klene, C. Adamo, R. Cammi, J. W. Ochterski, R. L. Martin, K. Morokuma, O. Farkas, J. B. Foresman and D. J. Fox, 2016. Gaussian, Inc., Wallingford CT.

(2) P. J. Stephens, F. J. Devlin, C. F. Chabalowski and M. J. Frisch, *J. Phys. Chem.*, 1994, **98**, 11623-11627.

(3) J.-D. Chai and M. Head-Gordon, *Phys. Chem. Chem. Phys.* 2008, **10**, 6615-6620.

(4) F. Weigend and R. Ahlrichs, *Phys. Chem. Chem. Phys.* 2005, **7**, 3297-3305.

(5) W. Humphrey, A. Dalke and K. Schulten, *J. Mol. Graph. Model.* 1996, **14**, 33-38.

(6) T. Lu and F. Chen, *J. Comput. Chem.*, 2012, **33**, 580-592.

(7) T. Lu and Q.Chen, *J. Comput. Chem.*, 2022, **43**, 539-555.

(8) T. L. Wu, M. J. Huang, C. C. Lin, P. Y. Huang, T. Y. Chou, R. W. Chen-Cheng, H. W. Lin, R. S. Liu and C. H. Cheng, *Nat. Photon*., 2018, **12**, 235-240.

(9) Q. Zhang, H. Kuwabara, W. J. Potscavage, Jr., S. Huang, Y. Hatae, T. Shibata and C. Adachi, *J. Am. Chem. Soc.*, 2014, **136**, 18070-18081.
(10) Q. Zhang, B. Li, S. Huang, H. Nomura, H. Tanaka and C. Adachi, *Nat. Photon.*, 2014, **8**, 326-332.
(11) H. J. Tan, G. X. Yang, Y. L. Deng, C. Cao, J. H. Tan, Z. L. Zhu, W. C. Chen, Y. Xiong, J. X. Jian, C. S. Lee and Q. X. Tong, *Adv. Mater.*, 2022, **34**, 2200537.